Coverage and Rate Analysis for Millimeter Wave Cellular Networks

Tianyang Bai and Robert W. Heath, Jr.

arXiv:1402.6430v2 [cs.IT] 1 Mar 2014

Abstract

Millimeter wave (mmWave) holds promise as a carrier frequency for fifth generation cellular networks. As mmWave signals are sensitive to blockage, prior microwave network models do not apply to analyze mmWave systems directly. Leveraging concepts from stochastic geometry, this paper proposes a general framework to evaluate the coverage and rate performance in mmWave cellular networks. Using a distance-dependent line-of-site (LOS) probability function, the locations of the LOS and non-LOS base stations as modeled as two independent non-homogeneous Poisson point processes, to which different path loss laws are applied. Based on the proposed framework, expressions for the signal-to-noise-and-interference ratio (SINR) and rate coverage probability are derived. The mmWave coverage and rate performance are examined as a function of the antenna geometry and base station density. The case of dense networks are further analyzed by applying a simplified system model, in which the LOS region of a user is approximated as a fixed LOS ball. The results show that dense mmWave networks can achieve comparable coverage and much higher data rates than microwave systems, despite the presence of blockages. The analysis also suggests that increasing base station density beyond a critical point (called the super dense regime) will harm the SINR and rate performance and that the cell size to achieve best optimal SINR scales with the average size of the area unblocked by blockages to a user.

I. Introduction

The large available bandwidth at millimeter wave (mmWave) frequencies makes them attractive for fifth generation cellular networks [3]–[5]. The mmWave band ranging from 3 GHz to 300 GHz

The authors are with The University of Texas at Austin, Austin, TX, USA. (email: tybai@utexas.edu, rheath@utexas.edu)
This work is supported in part by the National Science Foundation under Grant No. 1218338 and 1319556. Preliminary results related to this paper were presented at the 1st IEEE Global Conference on Signal and Information Processing (GlobalSIP) [1] and the 47th Annual Asilomar Conference on Signals, Systems, and Computers (Asilomar) [2].

has already been considered in various commercial wireless systems including IEEE 802.15.3c for personal area networking [6], IEEE 802.11ad for local area networking [7], and IEEE 802.16.1 for fixed-point access links [8]. Recent field measurements reveal the promise of mmWave signals for the access link (between the mobile station and base station) in cellular systems [5], [9].

One differentiating feature of mmWave cellular communication is the use of antenna arrays at the transmitter and receiver to provide array gain. As the wavelength decreases, antenna sizes also decrease reducing the antenna aperture. For example, from the Friis free-space equation [10], a mmWave signal at 20 GHz will experience 20 dB larger path loss than a microwave signal at 2 GHz. Thanks to the small wavelength, however, it is possible to pack multiple antenna elements into the limited space at mmWave transceivers [3]. With large antenna arrays, mmWave cellular systems can implement beamforming at the transmitter and receiver to provide array gain that compensates for the frequency-dependent path loss, overcomes additional noise power, and as a bonus also reduces out-of-cell interference [4].

Another distinguishing feature of mmWave cellular communication is the propagation environment. For example, mmWave signals are more sensitive to blockage effects than microwave signals, as certain materials like concrete walls found on building exteriors, causes severe penetration loss [11]. This indicates that indoor users are unlikely to be covered by outdoor mmWave base stations. Channel measurements using directional antennas [5], [9], [12] have revealed another interesting behavior at mmWave: blockages cause substantial differences in the line-of-sight (LOS) paths and non-line-of-sight (NLOS) path loss characteristics. Such differences have also been observed in microwave propagation studies, e.g. see [13]. The differences, however, become more significant for mmWave; as diffraction effects are negligible [4], there are only a few scattering clusters [14], and the angle spreads tend to be small [5], [14]. Measurements in [5], [9], [12] showed that mmWave signals propagate as in free space with a path loss exponent of 2. The situation was different for NLOS paths where a log distance model was fit with a higher path loss exponent and additional shadowing [5], [9]. The NLOS path loss laws tend to be more dependent on the scattering environment. For example, an exponent as large as 5.76 was found in downtown New York City [5], while only 3.86 was found on the UT Austin campus [9]. The distinguishing features of the propagation environment need to be incorporated into the any comprehensive system analysis of mmWave networks.

The performance of mmWave cellular networks was simulated in prior work [14], [15] using

insights from propagation channel measurements [5]. In [15], using the NLOS path loss law measured in the New York City, lower bounds of the signal-to-noise-and-interference ratio (SINR) distribution and the achievable rate were simulated in a 28 GHz pico-cellular system. In [14], a mmWave channel model that incorporated blockage effects and angle spread was proposed and further applied to simulate the mmWave network capacity. Both results in [14], [15] show that the achievable rate in mmWave networks can outperform microwave cellular networks by an order-of-magnitude. The simulation-based approach [14], [15] does not lead to elegant system analysis as in [16], which can be broadly applied to different deployment scenarios.

Stochastic geometry is a useful tool to analyze system performance in microwave cellular networks [16], [17]. In [16], by modeling base station locations in microwave networks as a Poisson point process (PPP) on the plane, the aggregate coverage probability was derived in closed form and shown to be as accurate as using the hexagonal grid model. There have been several extensions of the results in [16], such as analyzing a multi-tier network in [18] and predicting the site-specific performance in heterogeneous networks in [19]. It is not possible to directly apply results from microwave networks to mmWave networks due to the different propagation characteristics and the use of directional beamforming. There has been limited application of stochastic geometry to study mmWave cellular networks. The primary related work was in [20], where directional beamforming was incorporated for single and multiple user configurations, but a simplified path loss model was used that did not take mmWave propagation features into account.

A systematic study of mmWave network performance should incorporate the impact of blockages such as buildings in urban areas. One approach is to model the blockages explicitly in terms of their sizes, locations, and shapes using data from a geographic information system. This approach is well suited for site-specific simulations [21] using electromagnetic simulation tools like ray tracing [22]. An alternative is to employ a stochastic blockage model, e.g. [23], [24], where the blockage parameters are drawn randomly according to some distribution. The stochastic approach lends itself better to system analysis and can be applied to study system deployments under a variety of blockage parameters such as size and density.

The main contribution of this paper is to propose a stochastic geometry framework for analyzing the coverage and rate in mmWave cellular networks. As a byproduct, the framework also applies to analyze heterogenous networks in which the base stations are distributed as certain

non-homogeneous PPPs.We incorporate directional beamforming by modeling the steering orientations of the beamforming as marks of the base station PPPs. For tractability of the analysis, the actual beamforming patterns are also approximated by a sectored model, which characterizes key features of an antenna pattern: directivity gain, half-power beamwidth, and front-back ratio. A similar model was also employed in work on ad hoc networks [25]. To incorporate blockage effects, we model the probability that a communication link is LOS as a function of the link length, and provide a stochastic characterization of the region unblocked by blockages to a user, which we define as the *LOS region*. Applying the distance-dependent LOS probability function, the base stations are equivalently divided into two independent non-homogenous point processes on the plane, i.e., the LOS and the NLOS base station processes. Different path loss laws and fading are applied separably to the LOS and NLOS case. Based on the system model, expressions for the SINR and rate coverage probability are derived in general mmWave networks. To simplify the analysis, we also propose a systematic approach to approximate a complicated LOS function as its equivalent step function. Our analysis indicates that the coverage and rate performance is sensitive to the density of base stations and the distribution of blockages in mmWave networks, and that dense mmWave networks can generally achieve good coverage and significantly higher achievable rate than conventional cellular networks.

A simplified system model is proposed to analyze dense mmWave networks, where the infrastructure density is comparable to the blockage density. For a general LOS function, the LOS region observed by a user may have a random and unusual shape. Coverage analysis then requires integrating the SINR over this irregular coverage region [1]. We propose to simplify the analysis by approximating the actual LOS region as a fixed-sized ball defined as the *equivalent LOS ball*. With the simplified network model, we find that in a dense mmWave network, the cell size should scale with the size of LOS region to maintain the same coverage probability. We find that continuing to increase density (leading to what we call ultra-dense networks) that increasing base station density does not always improve SINR, and the optimal base station density should be finite.

Compared with our prior work in [1], this paper provides a generalized mathematical framework and includes the detailed mathematical derivations. The system model applies for a general LOS probability function and includes the impact of general small-scale fading. We also provide a new approach to compute coverage probability, which avoids inverting the Fourier transform

numerically and is more efficient than prior expressions in [1]. Compared with our prior work in [2], we also remove the constraint that the LOS path loss exponent is 2, and extend the results in [2] to general path loss exponents, in addition to providing derivations for all results, and new simulation results.

This paper is organized as follows. We introduce the system model in Section II. We derive expressions for the SINR and rate coverage in a general mmWave network in Section III. A systematic approach is also proposed to approximate general LOS probability functions as a step function to further simplify analysis. In Section IV, we apply the simplified system model to analyze performance and examine asymptotic trends in dense mmWave networks, where outdoor users observe more than one LOS base stations with high probability. Finally, conclusions and suggestions for future work are provided in Section V.

II. System Model

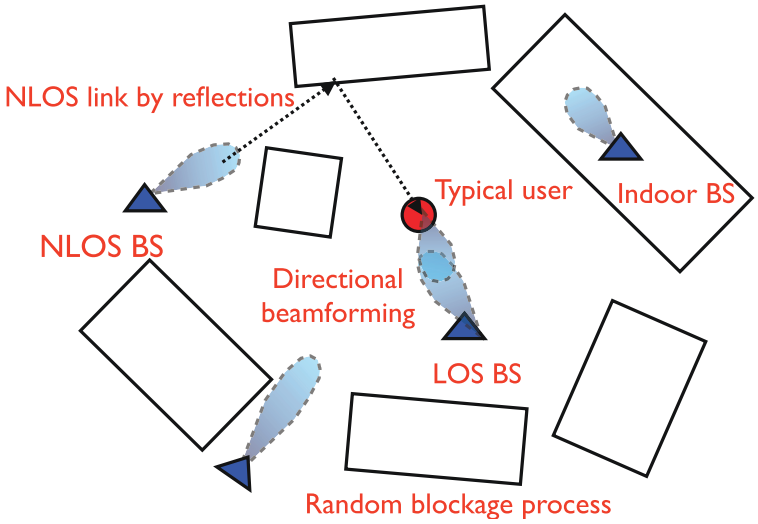

Fig. 1. A system model for a mmWave cellular network. Blockages are modeled as a random process of rectangles, while base stations are assumed to be distributed as a Poisson point process on the plane. An outdoor typical user is fixed at the origin, and the base stations can be categorized into three groups: indoor base stations, outdoor base stations that is LOS to the typical user, and outdoor base station NLOS to the user. Directional beamforming is performed at both base stations and mobile stations to exploit directivity gains.

In this section, we introduce our system model for evaluating the performance of a mmWave network. We focus on the downlink coverage and rate performance experienced by an outdoor

user, as illustrated in Fig. 1. We make the following assumptions when formulating the system model.

Assumption 1 (Blockage process): The blockages, typically buildings in urban areas, form a stationary process of random shapes, e.g. a Boolean scheme of rectangles [24], on the plane. Let τ denote the average fraction of the land covered by buildings in the network.

Assumption 2 (PPP BS): The base stations form a homogeneous PPP $\tilde{\Phi}$ with density $\tilde{\lambda}$ on the plane. All base stations are assumed to have a constant transmit power P_{t}. Note that a base station can be located either inside a building or outside a building. Let $\Phi = \{X_\ell\}$ be the point process of outdoor base stations, X_ℓ the ℓ-th outdoor base station, and $R_\ell = |OX_\ell|$ denote the distance from ℓ-th base station to the origin O. By the stationarity of the base station process, the equivalent density of the outdoor base stations is $\lambda = \tau\tilde{\lambda}$.

Assumption 3 (Outdoor user): An outdoor typical user is assumed to be located at the origin O, which is a standard approach in the analysis using stochastic geometry thanks to Slivnyak's theorem [16], [26]. In this paper we assume that indoor-to-outdoor penetration loss is high enough such that an outdoor user can not receive any signal or interference from an indoor base station. Hence, we will focus on the outdoor base station process Φ. By the stationarity of both the base station process and the blockage process, the downlink performance experienced by the typical user equals the average performance in the network. Thus, we will investigate the SINR and rate distribution of the outdoor typical user being served by outdoor infrastructure. Extension to incorporate finite indoor-to-outdoor penetration loss and indoor users are an interesting topic of future work.

We say that a base station at X is *LOS* to the typical user at the origin O if and only if there is no blockage intersecting the link OX. Due to the presence of blockages, only a subset of the outdoor base stations Φ are LOS to the typical user.

Assumption 4 (LOS and NLOS BS): An outdoor base station can be either LOS or NLOS to the typical user. Let Φ_{L} be the point process of LOS base stations, and $\Phi_{\mathrm{N}} = \Phi/\Phi_{\mathrm{L}}$ be the process of NLOS base stations. Define the *LOS probability function* $p(R)$ as the probability that a link of length R is LOS. Noting the fact that the longer the link, the more likely it will be intersected by blockages, $p(R)$ is a non-increasing function of R. The NLOS probability of a link is $1 - p(R)$.

The LOS probability function in a network can be derived from field measurements [14]

or stochastic blockage models [23], [24], where the blockage parameters are characterized by some random distributions. For instance, when the blockages are modeled as a rectangle boolean scheme in [24], it follows that $p(R) = \mathrm{e}^{-\beta R}$, where β is a parameter determined by the density and the average size of the blockages, and $1/\beta$ is what we call the average LOS range of the network [24].

Note that the LOS probability for different links are not independent in reality. For instance, neighboring base stations might be blocked by a large building simultaneously. Taking account the correlations in shadowing generally makes the exact analysis difficult. Numerical results in [24], however, indicated that ignoring such correlations cause a minor loss of accuracy in the SINR evaluation. Hence, we make an independent shadowing assumption.

Assumption 5 (Independent shadowing): The correlations of shadowing between links are ignored, i.e. the LOS probability on each link is assumed to be independent.

By Assumption 5 and the thinning theorem of PPP [26], the outdoor base station process Φ is a PPP of density λ on the plane, and the LOS base station process Φ_{L} and the NLOS process Φ_{N} form two independent non-homogeneous PPP with the density functions $p(R)\lambda$ and $(1-p(R))\lambda$ in polar coordinates, respectively.

Assumption 6 (Path loss model): Different path loss laws are applied to LOS and NLOS links. Given a link has length R, its path loss gain $L(R)$ is computed as

$$L(R) = \mathbb{I}(p(R))C_{\mathrm{L}}R^{-\alpha_{\mathrm{L}}} + (1 - \mathbb{I}(p(R))C_{\mathrm{N}}R^{-\alpha_{\mathrm{N}}}, \tag{1}$$

where $\mathbb{I}(x)$ is a Bernoulli random variable with parameter x, α_{L}, α_{N} are the LOS and NLOS path loss exponents, and C_{L}, C_{N} are the intercepts of the LOS and NLOS path loss formulas. Typical values of mmWave path loss exponents and intercept constants are available in prior work, see e.g. [5], [9].

Assumption 7 (Directional beamforming): Antenna arrays are deployed at both base stations and mobile stations to perform directional beamforming. Let $A_\ell = G_{\mathrm{r}}(\psi_{\mathrm{r}}^\ell)G_{\mathrm{t}}(\psi_{\mathrm{t}}^\ell)$ be the directivity gain of the link from the ℓ-th base station to the typical user, where $G_{\mathrm{r}}(\cdot)$ and $G_{\mathrm{t}}(\cdot)$ denote the antenna patterns at the receivers and the transmitters, ψ_{r}^ℓ and ψ_{t}^ℓ are the angle of arrival and the angle of departure of the signal from the ℓ-th base station.

Assumption 8 (Sector antenna pattern): For tractability of the analysis, the actual array patterns are approximated by a sectored antenna model, which was used in the ad hoc network

analysis [25]. As shown in Fig. 2, the array gains are assumed to be constant M for all angles in the main lobe, and another constant m in the side lobe in the sectored model. Let $G_{M,m,\theta}(\psi)$ be the directivity gain function of the sector antenna in Fig. 2, where θ is the beam width of the main lobe, and ψ is the angle off the boresight direction. The sectored model captures key features of an antenna pattern: the directivity gain, the front-to-back ratio (FBR), and the half-power beamwidth. We will use the sectored antenna patterns $G_{M_{\rm r},m_{\rm r},\theta_{\rm r}}(\cdot)$ and $G_{M_{\rm t},m_{\rm t},\theta_{\rm t}}(\cdot)$ to approximate the receiver and transmitter beamforming patterns $G_{\rm r}(\cdot)$ and $G_{\rm t}(\cdot)$ in the analysis.

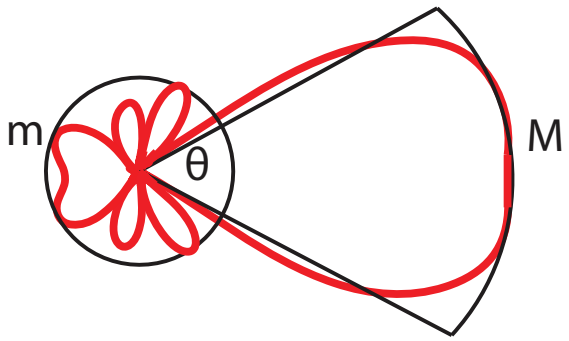

Fig. 2. The sectored antenna model $G_{M,m,\theta}$ used to approximate the beamforming pattern.

Assumption 9 (User association): The typical user is associated with the base station that has the smallest path loss. The serving base station is denoted as X_0. Both the mobile station and its serving base station will estimate channels including angles of arrivals and fading, and then adjust their antenna steering orientations accordingly to exploit the maximum directivity gain. Errors in channel estimation are neglected, and so as errors in time and carrier frequency synchronizations in our work. Thus, the directivity gain for the desired signal is $A_0 = M_{\rm r}M_{\rm t}$. For the ℓ-th interfering link, the angles $\psi_{\rm r}^{\ell}$ and $\psi_{\rm t}^{\ell}$ are independently and uniformly distributed in $(0, 2\pi]$, which gives a directivity gain of $A_\ell = G_{M_{\rm t},m_{\rm t},\theta_{\rm t}}(\psi_{\rm t}^{\ell})G_{M_{\rm r},m_{\rm r},\theta_{\rm r}}(\psi_{\rm r}^{\ell})$.

By Assumption 8 and Assumption 9, for an interference link, A_ℓ is a discrete random variable with the probability distribution as $A_\ell = a_k$ with probability b_k ($0 < k \leq 4$), where a_k and b_k are constants defined in Table I, $c_{\rm r} = \frac{\theta_{\rm r}}{2\pi}$, and $c_{\rm t} = \frac{\theta_{\rm t}}{2\pi}$.

Assumption 10 (Small-scale fading): We assume independent Nakagami fading for each link. Different parameters of Nakagami fading $N_{\rm L}$ and $N_{\rm N}$ are assumed for LOS and NLOS links. Let

TABLE I

PROBABILITY MASS FUNCTION OF A_ℓ AND D_ℓ

k	1	2	3	4
b_k	$c_{\mathrm{r}}c_{\mathrm{t}}$	$c_{\mathrm{r}}(1-c_{\mathrm{t}})$	$(1-c_{\mathrm{r}})c_{\mathrm{t}}$	$(1-c_{\mathrm{r}})(1-c_{\mathrm{t}})$
a_k	$M_{\mathrm{r}}M_{\mathrm{t}}$	$M_{\mathrm{r}}m_{\mathrm{t}}$	$m_{\mathrm{r}}M_{\mathrm{t}}$	$m_{\mathrm{r}}m_{\mathrm{t}}$
f_k	M_{r}	$M_{\mathrm{r}}\xi_{\mathrm{t}}$	m_{r}	$m_{\mathrm{r}}\xi_{\mathrm{t}}$

h_ℓ be the small-scale fading term on the ℓ-th link. Then $|h_\ell|^2$ is a normalized gamma random variable. Further, for simplicity, we assume N_{L} and N_{N} are positive integers. We also ignore the frequency selectivity in fading, as measurements show that the delay spread is generally small [5], and the impact of frequency-selective fading can be minimized by techniques like orthogonal frequency-division multiplexing (OFDM) or frequency domain equalization [10].

Measurement results indicated that small-scale fading at mmWave is less severe than at mmWave systems when narrow beam antennas are used [5]. We use a large Nakagami parameter N to approximate small-variance fading as found in the LOS case for example. Let σ^2 be the thermal noise power normalized by P_{t}. Based on the assumptions thus far, the SINR received by the typical user can be expressed as

$$\text{SINR} = \frac{|h_0|^2 M_{\mathrm{r}} M_{\mathrm{t}} L(R_0)}{\sigma^2 + \sum_{\ell>0: X_\ell \in \Phi} |h_\ell|^2 A_\ell L(R_\ell)}. \tag{2}$$

Using the proposed system model, we will evaluate the mmWave SINR and rate coverage in the following section.

III. COVERAGE AND RATE ANALYSIS IN GENERAL NETWORKS

In this section, we analyze the coverage and rate in a general mmWave network. First, we provide some SINR ordering results regarding different parameters of the antenna pattern. Then we derive expressions for the SINR and rate coverage probability in mmWave networks with general LOS probability function $p(R)$. To simplify subsequent analysis, we then introduce a systematic approach to approximate $p(R)$ by a moment matched equivalent step function. Finally, we provide numerical results to provide insights into the importance of density in achieving high coverage and rate in mmWave networks.

A. SINR Ordering with Different Array Geometry

One differentiating feature of mmWave cellular networks is the deployment of directional antenna arrays. Consequently, the performance of mmWave networks will depend on the adaptive array pattern through the beam width, directivity gain, and the FBR. In this section we establish some results on SINR ordering as a function of the parameters of the pattern focusing on the array geometry at the transmitter. The same ordering results, however, also apply to the receiver array geometry.

Let the FBR at the transmitter be defined as the ratio between the main lobe directivity gain M_{t} and the back lobe gain m_{t}, denoted as $\xi_{\mathrm{t}} = M_{\mathrm{t}}/m_{\mathrm{t}}$. Now we introduce a key result on ordering of the SINR with respect to the directivity.

Proposition 1 (SINR ordering w.r.t. directivity gains): With fixed beamwidth θ_{t} and FBR ξ_{t} at the transmitter , the SINR increases as the main lobe directivity gain M_{t} increases. Similarly, with fixed beamwidth θ_{t} and main lobe gain M_{t} , the SINR increases as the FBR ξ_{t} increases.

Proof: Normalizing both the numerator and denominator by M_t, we can express the SINR as $\mathrm{SINR} = \frac{|h_0|^2 M_{\mathrm{r}} L(R_0)}{\sigma^2/M_{\mathrm{t}} + \sum_{\ell>0: X_\ell \in \Phi} D_\ell(\xi_{\mathrm{t}})|h_\ell|^2 L(R_\ell)}$, where $D_\ell(\xi_{\mathrm{t}}) = d_k$ with probability b_k, and b_k, f_k are constants defined in Table I. $D_\ell(\xi_{\mathrm{t}})$ is independent of M_{t}, and is a non-increasing function of ξ_{t}. Hence, when ξ_{t} is fixed, larger M_{t} provides larger SINR; when M_{t} is fixed, larger ξ_{t} provides larger SINR. ■

Next, we provide the ordering results regarding beam width as follows.

Proposition 2 (SINR ordering w.r.t. beam width): Given the main lobe gain M_{t} and the FBR ξ_{t} at the transmitter, smaller beamwidth θ_{t} provides better SINR.

The proposition can be rigorously proved using coupling techniques. We omit the proof here and instead provide an intuitive explanation as below. Intuitively, with narrower main lobes, fewer base stations will transmit interference to the typical user via their main lobes, which gives a smaller interference power. The desired signal term in (2) is independent of the beamwidth, as we ignore the channel estimation errors and potential angle spreads.Hence, based on our model assumptions, smaller beamwidths provide a better SINR performance.

We note that the ordering result in Proposition 2 assumes that there is no angle spread in the channel. With angle spread, a narrow-beam antenna may capture only the signal energy arriving inside its main lobe, and miss the energy spread outside, which causes a gain reduction in the signal power [27]. Consequently, the results should be interpreted as applying to the case

where beamwidths are larger than the angle spread, e.g. the measurement using antennas with a beamwidth of 55° in [12]. We defer more detailed treatment of angle spread to future work.

B. SINR Coverage Analysis

In this section, we derive expressions for the SINR coverage probability in mmWave cellular networks. The SINR coverage probability $P_{\mathrm{c}}(T)$ is defined as the probability that the received SINR is larger than some threshold $T > 0$, i.e., $P_{\mathrm{c}}(T) = \mathbb{P}(\text{SINR} > T)$.

We present the following lemmas before introducing the main results on SINR coverage. By Assumption 4, the outdoor base station process Φ can be divided into two independent non-homogeneous PPPs: the LOS base station process Φ_{L} and NLOS process Φ_{N}. We will equivalently consider Φ_{L} and Φ_{N} as two independent tiers of base stations. As the user is assumed to connect to the base station with the smallest path loss, the serving base station can only be either the nearest base station in Φ_{L} or the nearest one in Φ_{N}. The following lemma provides the distribution of the distance to the nearest base station in Φ_{L} and Φ_{N}.

Lemma 1: The probability density function of the distance from an outdoor user to the nearest LOS base station is

$$f_{\mathrm{L}}(x) = 2\pi\lambda x p(x) \mathrm{e}^{-2\pi\lambda \int_0^x r p(r) \mathrm{d}r}. \tag{3}$$

The probability density function of the distance to the nearest NLOS base station is

$$f_{\mathrm{N}}(x) = 2\pi\lambda x (1 - p(x)) \mathrm{e}^{-2\pi\lambda \int_0^x r (1-p(r)) \mathrm{d}r}, \tag{4}$$

where $x > 0$, and $p(r)$ is the LOS probability function defined in Section II.

Proof: The proof follows [24, Theorem 10] and is omitted here. ■

Next, we compute the probability that the typical user is associated with a LOS or a NLOS base station as follows.

Lemma 2: The probability that the user is associated with a LOS base station is

$$A_{\mathrm{L}} = \int_0^\infty \mathrm{e}^{-2\pi\lambda \int_0^{\psi_{\mathrm{L}}(x)} (1-p(t)) t \mathrm{d}t} f_{\mathrm{L}}(x) \mathrm{d}x, \tag{5}$$

where $\psi_{\mathrm{L}}(x) = \left(C_{\mathrm{N}}/C_{\mathrm{L}}\right)^{1/\alpha_{\mathrm{N}}} x^{\alpha_{\mathrm{L}}/\alpha_{\mathrm{N}}}$. The probability that the user is associated with a NLOS base station is $A_{\mathrm{N}} = 1 - A_{\mathrm{L}}$.

Proof: See Appendix B. ■

Further, conditioning on that the serving base station is LOS (or NLOS), the distance from the user to its serving base station follows the distribution given in the following lemma.

Lemma 3: Given that a user is associated with a LOS base station, the probability density function of the distance to its serving base station is

$$\hat{f}_{\mathrm{L}}(x) = \frac{f_{\mathrm{L}}(x)}{A_{\mathrm{L}}} \mathrm{e}^{-2\pi\lambda \int_0^{\psi_{\mathrm{L}}(x)} (1-p(t))t\mathrm{d}t}, \tag{6}$$

when $x > 0$. Given the user is served by a NLOS base station, the probability density function of its distance to the serving base station is

$$\hat{f}_{\mathrm{N}}(x) = \frac{f_{\mathrm{N}}(x)}{A_{\mathrm{N}}} \mathrm{e}^{-2\pi\lambda \int_0^{\psi_{\mathrm{N}}(x)} p(t)t\mathrm{d}t}, \tag{7}$$

where $x > 0$, and $\psi_{\mathrm{N}}(x) = (C_{\mathrm{L}}/C_{\mathrm{N}})^{1/\alpha_{\mathrm{L}}}\, x^{\alpha_{\mathrm{N}}/\alpha_{\mathrm{L}}}$.

Proof: The proof follows a similar method as that of Lemma 2, and is omitted here. ■

Now, based on Lemma 2 and Lemma 3, we present the main theorem on the SINR coverage probability as follows

Theorem 3: The SINR coverage probability $P_c(T)$ can be computed as

$$P_{\mathrm{c}}(T) = A_{\mathrm{L}} P_{\mathrm{c,L}}(T) + A_{\mathrm{N}} P_{\mathrm{c,N}}(T), \tag{8}$$

where for $\mathrm{s} \in \{\mathrm{L}, \mathrm{N}\}$, $P_{\mathrm{c},s}(T)$ is the conditional coverage probability given that the user is associated with a base station in Φ_{s}. Further, $P_{\mathrm{c,s}}(T)$ can be evaluated as

$$P_{c,\mathrm{L}}(T) \approx \sum_{n=1}^{N_{\mathrm{L}}} (-1)^{n+1} \binom{N_{\mathrm{L}}}{n} \int_0^{\infty} \mathrm{e}^{-\frac{n\eta_{\mathrm{L}} x^{\alpha_{\mathrm{L}}} T\sigma^2}{C_{\mathrm{L}} M_{\mathrm{r}} M_{\mathrm{t}}} - Q_n(T,x) - V_n(T,x)} \hat{f}_{\mathrm{L}}(x)\mathrm{d}x, \tag{9}$$

and

$$P_{c,\mathrm{N}}(T) \approx \sum_{n=1}^{N_{\mathrm{N}}} (-1)^{n+1} \binom{N_{\mathrm{N}}}{n} \int_0^{\infty} \mathrm{e}^{-\frac{n\eta_{\mathrm{N}} x^{\alpha_{\mathrm{N}}} T\sigma^2}{C_{\mathrm{N}} M_{\mathrm{r}} M_{\mathrm{t}}} - W_n(T,x) - Z_n(T,x)} \hat{f}_{\mathrm{N}}(x)\mathrm{d}x. \tag{10}$$

where

$$Q_n(T,x) = 2\pi\lambda \sum_{k=1}^{4} b_k \int_x^{\infty} f\left(N_{\mathrm{L}}, \frac{n\eta_{\mathrm{L}} \bar{a}_k T x^{\alpha_{\mathrm{L}}}}{N_{\mathrm{L}} t^{\alpha_{\mathrm{L}}}}\right) p(t)t\mathrm{d}t, \tag{11}$$

$$V_n(T,x) = 2\pi\lambda \sum_{k=1}^{4} b_k \int_{\psi_{\mathrm{L}}(x)}^{\infty} f\left(N_{\mathrm{N}}, \frac{nC_{\mathrm{N}}\eta_{\mathrm{L}} \bar{a}_k T x^{\alpha_{\mathrm{L}}}}{C_{\mathrm{L}} N_{\mathrm{N}} t^{\alpha_{\mathrm{N}}}}\right) (1-p(t))t\mathrm{d}t, \tag{12}$$

$$W_n(T,x) = 2\pi\lambda \sum_{k=1}^{4} b_k \int_{\psi_{\mathrm{N}}(x)}^{\infty} f\left(N_{\mathrm{L}}, \frac{nC_{\mathrm{L}}\eta_{\mathrm{N}} \bar{a}_k T x^{\alpha_{\mathrm{N}}}}{C_{\mathrm{N}} N_{\mathrm{L}} t^{\alpha_{\mathrm{L}}}}\right) p(t)t\mathrm{d}t, \tag{13}$$

$$Z_n(T,x) = 2\pi\lambda \sum_{k=1}^{4} b_k \int_x^{\infty} f\left(N_{\mathrm{N}}, \frac{n\eta_{\mathrm{N}} \bar{a}_k T x^{\alpha_{\mathrm{N}}}}{N_{\mathrm{N}} t^{\alpha_{\mathrm{N}}}}\right) (1-p(t))t\mathrm{d}t, \tag{14}$$

and $f(N,x) = 1 - 1/(1+x)^N$. For $s \in \{\mathrm{L}, \mathrm{N}\}$, $\eta_s = N_s(N_s!)^{-\frac{1}{N_s}}$, N_s are the parameters of the Nakagami small-scale fading; for $1 \leq k \leq 4$, $\bar{a}_k = \frac{a_k}{M_\mathrm{t} M_\mathrm{r}}$, a_k and b_k are constants defined in Table I.

Proof: See Appendix D. ■

Though as an approximation of the SINR coverage probability, we will later show that the expressions in Theorem 3 are comparable to the simulations in Section III-E. More importantly, the expressions in Theorem 3 compute much more efficiently than prior results in [1], which required inverting Fourier transform numerically. Last, the LOS probability function $p(t)$ may itself have a very complicated form, e.g. the empirical function for small cell simulations in [13], which will make the numerical evaluation difficult. Hence, we propose simplifying the system model by using a step function to approximate $p(t)$ in Section III-D. Before that, we introduce our rate analysis results in the following section.

C. Rate Analysis

In this section, we analyze the distribution of the achievable rate Γ in mmWave networks. We use the following definition for the achievable rate

$$\Gamma = W \log_2(1 + \min\{\mathrm{SINR}, D\}), \tag{15}$$

where W is the bandwidth assigned to the typical user, and D is a SINR threshold determined by the order of the constellation and potential distortions from the RF circuit. The use of a distortion threshold D is needed because of the potential for very high SINRs in mmWave that may not be exploited due to other limiting factors like linearity in the radio frequency front end.

The average achievable rate $\mathbb{E}[\Gamma]$ can be computed using the following Lemma from the SINR coverage probability $P_\mathrm{c}(T)$.

Lemma 4: Given the SINR coverage probability $P_\mathrm{c}(T)$, the average achievable rate in the network is $\mathbb{E}[\Gamma] = \frac{W}{\ln 2} \int_0^D \frac{P_\mathrm{c}}{1+T} \mathrm{d}T$.

Proof: See [16, Theorem 3] and [20, Section V]. ■

Lemma 4 provides a first order characterization of the rate distribution. We can also derive the exact rate distribution using the *rate coverage probability* $P_\mathrm{R}(\gamma)$, which is the probability that the achievable rate of the typical user is larger than some threshold γ: $P_\mathrm{R}(\gamma) = \mathbb{P}[\Gamma > \gamma]$.

The rate coverage probability $P_{\mathrm{R}}(\gamma)$ can be evaluated through a change of variables as in the following lemma.

Lemma 5: Given the SINR coverage probability $P_{\mathrm{c}}(T)$, for $\gamma < W \log_{\mathrm{N}}(1+D)$, the rate coverage probability can be computed as $P_{\mathrm{R}}(\gamma) = P_{\mathrm{c}}(2^{\gamma/W}-1)$.

Proof: The proof is similar to that of [28, Theorem 1]. For $\gamma < W \log_{\mathrm{N}}(1+D)$, it directly follows that $P_{\mathrm{R}}(\gamma) = \mathbb{P}\left[\mathrm{SINR} > 2^{\gamma/W}-1\right] = P_{\mathrm{c}}(2^{\gamma/W}-1)$. ■

Using the rate distribution will allow comparisons to be made between mWave rates and microwave systems that use different bandwidths as presented in Section III-E.

D. Simplification of LOS Probability Function

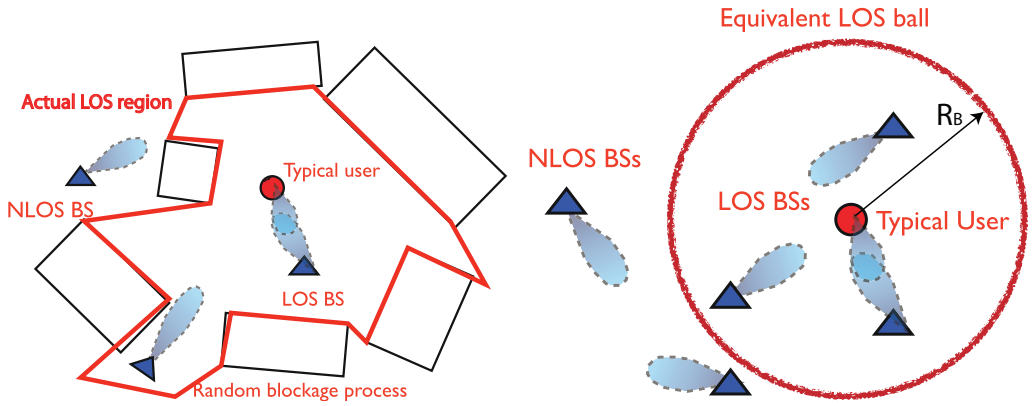

(a) Irregular shape of an acutal LOS region. (b) Approximation using the equivalent LOS ball.

Fig. 3. Simplification of the random LOS region as a fixed equivalent LOS ball. In (a), we illustrate one realization of random located buildings corresponding to a general LOS function $p(x)$. The LOS region observed by the typical user is an irregular polygon. In (b), we approximate $p(x)$ by a step function. Equivalently, the LOS region is also approximated by a fixed ball. Only base stations inside the ball are considered LOS to the user.

The expressions in Theorem 3 generally require computing multiple integrals numerically, and may become difficult to analyze. In this section, we propose to simplify the analysis by approximating a general LOS probability function $p(t)$ by a step function. We denote the step function as $S_{R_{\mathrm{B}}}(x)$, where $S_{R_{\mathrm{B}}}(x) = 1$ when $0 < x < R_{\mathrm{B}}$, and $S_{R_{\mathrm{B}}}(x) = 0$ otherwise. Essentially, the LOS probability of the link is taken to be one within a certain fixed radius R_{B} and zero outside the radius. An interpretation of the simplification is that the irregular geometry of the LOS region in Fig. 3 (a) is replaced with its equivalent LOS ball in Fig. 3

(b). Such simplification not only provides efficient expressions to compute SINR, but enables simpler analysis of the network performance when the network is dense.

We will propose two criterions to determine the R_{B} given LOS probability function $p(t)$. Before that, we first review some useful facts.

Theorem 4: Given the LOS probability function $p(x)$, the average number of LOS base stations that a typical user may observe is $\rho = 2\pi\lambda \int_0^\infty p(t)t\mathrm{d}t$.

Proof: The average number of LOS base stations can be computed as

$$\rho = \mathbb{E}\left[\sum_{X_\ell \in \Phi} \mathbb{I}(X_\ell \in \Phi_{\mathrm{L}})\right] \overset{(a)}{=} 2\pi\lambda \int_0^\infty p(t)t\mathrm{d}t,$$

where (a) follows directly from Compbell's formula of PPP [26]. ■

A direct corollary of Theorem 4 follows as below.

Corollary 4.1: When $p(x) = S_R(x)$, the average number of LOS base stations is $\rho = 2\pi\lambda R^2$.

Note that Theorem 4 also indicates that a typical user will observe a finite number of LOS base stations almost surely when $\int_0^\infty p(t)t\mathrm{d}t < \infty$. Hence, if $p(x)$ satisfies $\int_0^\infty p(t)t\mathrm{d}t < \infty$, the parameter R_{B} in $S_{R_{\mathrm{B}}}(x)$ can be determined by matching the average number of LOS base stations a user may observe as follows.

Criterion 1 (Mean LOS BS Number): When $\int_0^\infty p(t)t\mathrm{d}t < \infty$, the parameter R_{B} of the equivalent step function $S_{R_{\mathrm{B}}}(x)$ is determined to match the first moment of ρ. By Theorem 4, it follows that $R_{\mathrm{B}} = \left(2\int_0^\infty p(t)t\mathrm{d}t\right)^{0.5}$.

In the case where $\int_0^\infty p(t)t\mathrm{d}t < \infty$ is not satisfied, another criterion to determine R_{B} is needed. Note that even if the first moment is infinite, the probability that the user is associated with a LOS base station exists and is naturally finite for all $p(t)$. Hence, we propose the second criterion regarding the LOS association probability as follows.

Criterion 2 (LOS Association Probability): Given a LOS probability function $p(t)$, the parameter R_{B} of its equivalent step function $S_{R_{\mathrm{B}}}(x)$ is determined such that the LOS association probability A_{L} is unchanged after approximation.

From Lemma 2, the LOS association probability for a step function $S_{R_{\mathrm{B}}}(x)$ equals $1 - \mathrm{e}^{-\lambda\pi R_{\mathrm{B}}^2}$. Hence, by Criterion 2, R_{B} can be determined as $R_{\mathrm{B}} = \left(\frac{-\ln(1-A_{\mathrm{L}})}{\lambda\pi}\right)^{0.5}$.

Last, we explain the physical meaning of the step function approximation as follows. As shown in Fig. 3(a), with a general LOS probability function $p(x)$, the buildings are randomly located, and thus the actual LOS region observed by the typical user may have an unusual shape.

Although it is possible to incorporate such randomness of the size and shape by integrating over $p(t)$, the expressions with multiple integrals can make the analysis and numerical evaluation difficult [1]. In Fig. 3(b), by approximating the LOS probability function as a step function $S_{R_{\mathrm{B}}}(x)$, we equivalently approximate the LOS region by a fixed ball $\mathcal{B}(0, R_{\mathrm{B}})$, which we define as the *equivalent LOS ball*. As will be shown in Section IV, approximating $p(x)$ as a step function enables fast numerical computation, simplifies the analysis, and provides design insights for dense network. Besides, we will show in simulations below that the error due to such approximation is generally small in dense mmWave networks.

E. Validation and Discussions

In this section, we provide numerical results to validate our analytical results and further discuss their implications on system design. We assume the mmWave network is operated at 28 GHz, and the bandwidth assigned to each user is $W = 100$ MHz. The LOS and NLOS path loss exponent are $\alpha_{\mathrm{L}} = 2$ and $\alpha_{\mathrm{N}} = 4$. The parameters of the Nakagami fading are $N_{\mathrm{L}} = 3$ and $N_{\mathrm{N}} = 2$. We assume the LOS probability function is $p(x) = \mathrm{e}^{-\beta x}$, where $1/\beta = 141.4$ meters. For the ease of illustration, we denote the average cell radius as $r_{\mathrm{c}} = \sqrt{1/\pi\lambda}$.

First, we simulate the SINR coverage probability with different transmit antenna parameters. As shown in Fig. 4, when the side lobe gain m_{t} is fixed, better SINR performance is achieved by increasing main lobe gain M_{t} and by decreasing the main lobe beam width θ_{t}, as indicated by the ordering results in III-A.

Next, we compare network performance with different base station densities in Fig. 5. The results show that the probability that a user is associated with a LOS base station increases as the base station density grows, which also indicates the network performance will be mostly determined by the distribution of LOS base stations in a sufficiently dense network, e.g. when the average cell size is smaller than 100 meters in the simulation.

We also compare the SINR coverage probability with different base station densities in Fig. 6. The numerical results in Fig. 6 (a) show that our analytical results in Theorem 3 match the simulations well with negligible errors. Unlike in a interference-limited microwave network, where SINR is almost invariant with the base station density [16], the mmWave SINR coverage probability is also shown to be sensitive to the base station density in Fig. 6. The results in Fig. 6 (a) also shows that mmWave networks generally require a high base station density to

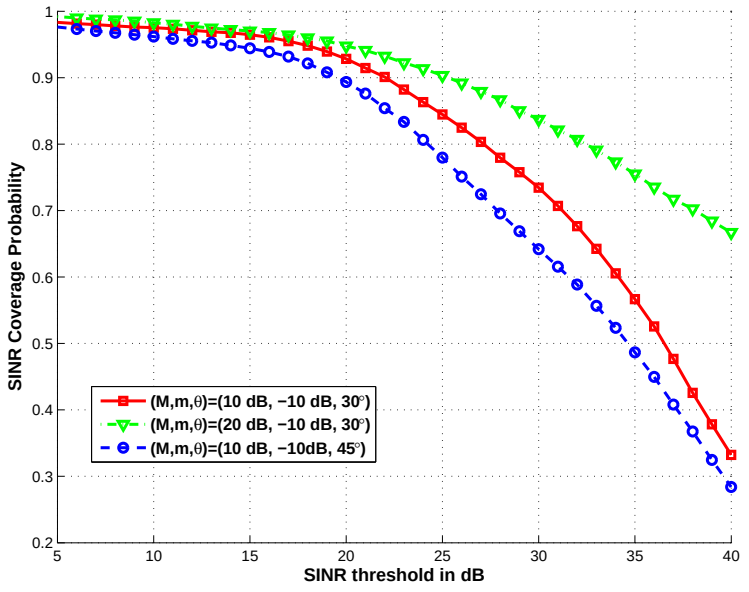

Fig. 4. SINR coverage probability with different antenna geometry. The average cell radius is $r_{\mathrm{c}} = 100$ meters. The receiver beam pattern is fixed as $G_{10\mathrm{dB},-10\mathrm{dB},90^\circ}$.

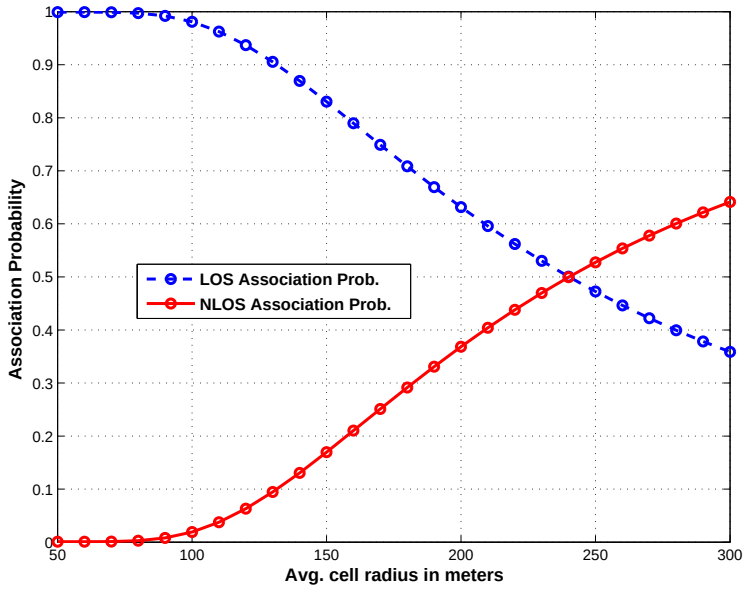

Fig. 5. LOS association probability with density base station densities.

achieve acceptable SINR coverage. Moreover, the results in Fig. 6 (b) show that with increasing base station density, mmWave networks will transit from power-limited regime into interference-

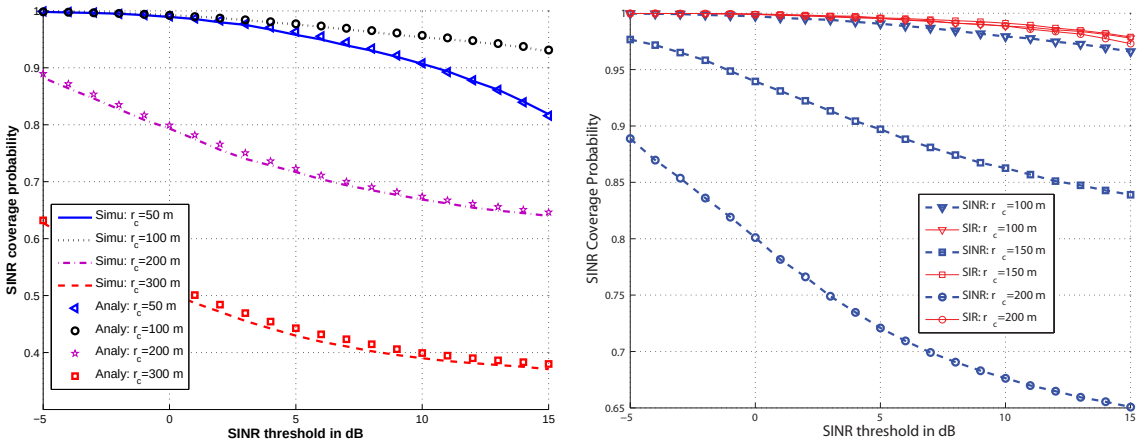

(a) Analytical bounds using Theorem 3. (b) Comparison between SINR and SIR.

Fig. 6. SINR coverage probability with different base station densities. The transmit antenna pattern is assumed to be $G_{100\text{dB},0\text{dB},30^\circ}$. In (a), analytical results from Theorem 3 are shown to provide a tight approximation. In (b), it shows that SIR converges to SINR when the base station density becomes high, which implies that mmWave networks can be interference-limited.

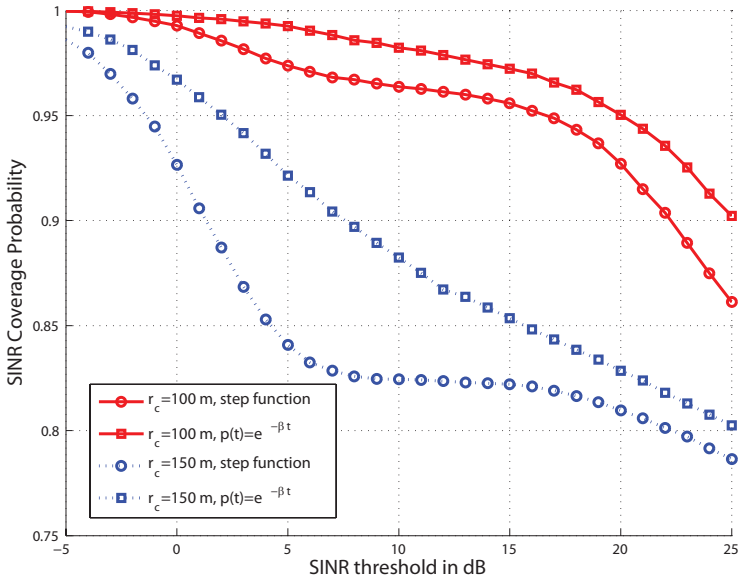

Fig. 7. Comparison of the SINR coverage between using $p(x)$ and its equivalent step function $S_{R_\text{B}}(x)$. The transmit antenna pattern is assumed to be $G_{20\text{dB},-10\text{dB},30^\circ}$. It shows that the step function tends to provide a more pessimistic SINR coverage probability, but the gap becomes smaller as the network becomes more dense

limited regime; as the SIR curves will converge to the SINR curve when densifying the network.

Specifically, comparing the curves for $r_c = 200$ meters and $r_c = 300$ meters in Fig. 6 (a),

we find that increasing base station density generally improve the SINR in a sparse network; as increasing base station density will increase the LOS association probability and avoid the presence of coverage holes, i.e. the cases that a user observes no LOS base stations. A comparison of the cases of $r_c = 100$ meters and $r_c = 50$ meters, however, also indicates that increasing base station density need not improve SINR, especially when the network is already sufficiently dense. Intuitively, increasing base station density also increases the likelihood to be interfered by strong LOS interferers. In a sufficiently dense network, increasing base station will harm the SINR by adding more strong interferers. Thus, the performance of dense mmWave networks can be improved by interference management, such as switching off some base stations with light load. We will later give a more strict mathematical explanation for this observation in Section IV-C.

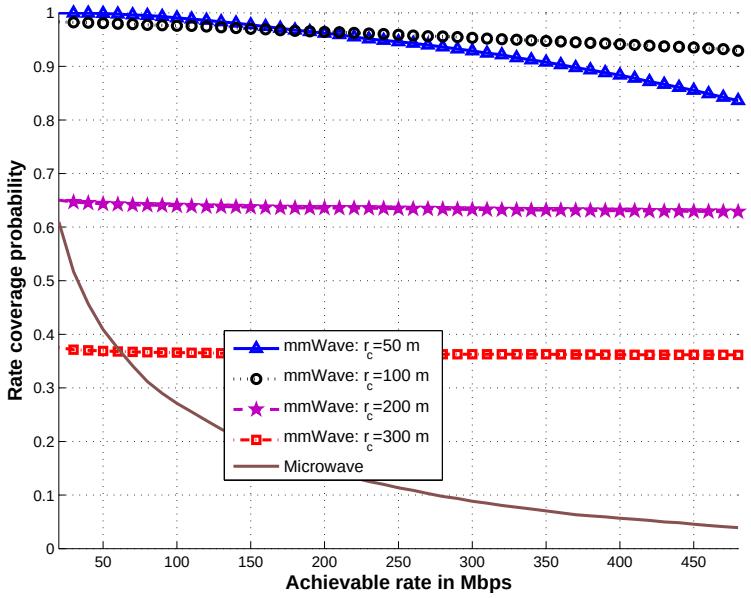

Fig. 8. Rate coverage comparison between mmWave and microwave cellular networks. The mmWave transmit antenna pattern is assumed to be $G_{10\text{dB},-10\text{dB},30^\circ}$. We assume the microwave system is operated at 2 GHz with a cell radius of 500 m, and the transmit power of the microwave base station is 46 dBm.

Now we compare the SINR coverage with different LOS probability functions $p(x)$. We approximate the negative exponential function $p(x) = \mathrm{e}^{-\beta x}$ by its equivalent step function $S_{R_\mathrm{B}}(x)$. Applying either of the criteria in Section III-D, the radius of the equivalent LOS ball R_B equals 200 meters. As shown in Fig. 7, the step function approximation generally provides

a lower bound of the actual SINR distribution, and the errors due to the approximation become smaller when the base station density increases. The approximation of step function also enables faster evaluations of the coverage probability, as it simplifies expressions for the numerical integrals. Thus, we propose to use this first-order approximation of the LOS probability function to simplify the analysis of dense networks in Section IV.

Last, simulate rates in a mmWave system. In the rate simulation, we assume that 64 QAM is the highest constellation supported in the networks, and thus the maximum spectrum efficiency per data stream is 6 bps/Hz. In Fig. 8, we compare the rate coverage probability between the mmWave network and a microwave network operated at 2 GHz. The microwave system has a signal bandwidth of 20 MHz, while the mmWave bandwidth is 100 MHz. Rayleigh fading is assumed in the microwave simulations. We further assume that microwave base stations have perfect channel state information, and apply spatial multiplexing (4×4 single user MIMO with zero-forcing precoder) to transmit multiple data streams. More comparison results with other techniques can be found in [29]. Results in Fig. 8 shows that, due to the larger available bandwidth at mmWave frequencies and favorable SINR distribution, the mmWave system outperforms the microwave system in terms of providing high data rate coverage.

IV. Analysis of Dense mmWave Networks

Our coverage analysis in the previous section showed that mmWave deployments will be dense if they are expected to achieve significant coverage. In this section we specialize our results to the dense scenario, obtaining simplified expressions for the SINR and further insights into system performance in this important asymptotic regime.

A. Dense Network Model

In this section, we build the dense network model by modifying the system model in Section II with a few additional assumptions. We say that a mmWave cellular network is *dense* if the average number of LOS base stations observed by the typical user ρ is larger than K, or if its LOS association probability A_{L} is larger than $1-\epsilon$, where K and ϵ are pre-defined positive thresholds. In this paper, for illustration purpose, we will let $K=1$ and $\epsilon=5\%$. Further, we say that a network is *ultra-dense* when $\rho>10$. Note that ρ also equals the relative base station density normalized by the average LOS area, as we will explain below.

Now we make some additional assumptions that will allow us to further simplify the network model.

Assumption 11 (LOS equivalent ball): The LOS region of the typical user is approximated by its equivalent LOS ball $\mathcal{B}(0, R_{\mathrm{B}})$ as defined in Section III-D.

By Assumption 11, the LOS probability function $p(t)$ is approximated by its equivalent step function $S_{R_{\mathrm{B}}}(x)$, and the LOS base stations Φ_{L} form a homogeneous PPP inside the LOS ball $\mathcal{B}(0, R_{\mathrm{B}})$. In this case, the average number of LOS base stations is $\rho = \lambda \pi R_{\mathrm{B}}^2$, which is the raw base station density times the area of the LOS region. For the ease of illustration, we call ρ the *the relative density* of a mmWave network. Essentially, the relative density ρ is equivalently: (i) the average number of LOS base stations that a user can observe, (ii) the ratio of the average LOS area πR_{B}^2 to the size of a typical cell $1/\lambda$ [26], and (iii) the normalized base station density by the size of the LOS ball. We will show in the next section that the SINR coverage in dense networks is largely determined by the relative density ρ.

Assumption 12 (No NLOS and noise): Both NLOS base stations and thermal noise are ignored in the analysis since in the dense regime, the performance is limited by other LOS interferers.

We show later in the simulations that ignoring NLOS base stations and the thermal noise introduces a negligible error in the performance evaluation.

Assumption 13 (No Small-scale fading): Small-scale fading is ignored in the dense network analysis, as the signal power from a nearby mmWave LOS transmitter is found to be almost deterministic in measurements [5].

Based on the dense network model, the signal-to-interference ratio (SIR) can be expressed as

$$\mathrm{SIR} = \frac{M_{\mathrm{t}} M_{\mathrm{r}} R_0^{-\alpha_{\mathrm{L}}}}{\sum_{\ell: X_\ell \in \Phi \cap \mathcal{B}(0, R_{\mathrm{B}})} A_\ell R_\ell^{-\alpha_{\mathrm{L}}}}. \tag{16}$$

Now we compute the SIR distribution in the dense network model.

B. Coverage Analysis in Dense Networks

In this section, we derive an approximation of the SINR distribution in a mmWave dense network. Our main result is summarized in the following theorem.

Theorem 5: The SINR coverage probability in a dense network can be approximated as

$$P_{\mathrm{c}}(T) \approx \rho \mathrm{e}^{-\rho} \sum_{\ell=1}^{N} (-1)^{\ell+1} \binom{N}{\ell} \int_0^1 \exp\left(-\frac{2}{\alpha_{\mathrm{L}}} b_k \left(\ell \eta T \bar{a}_k\right)^{\frac{2}{\alpha_{\mathrm{L}}}} \Gamma\left(-\frac{2}{\alpha_{\mathrm{L}}}; \ell \eta T \bar{a}_k, \ell \eta T \bar{a}_k s^{\frac{\alpha_{\mathrm{L}}}{2}} \right) \right) \mathrm{d}t, \tag{17}$$

where $\Gamma(s;a,b) = \int_a^b x^{s-1}\mathrm{e}^{-x}\mathrm{d}x$ is the incomplete gamma function, $\bar{a}_k = a_k/(M_{\mathrm{t}}M_{\mathrm{r}})$, a_k and b_k are defined in Table I, $\eta = N(N!)^{\frac{1}{N}}$, and N is the number of terms used in the approximation.

Proof: See Appendix D. ■

When $\alpha_{\mathrm{L}} = 2$, the expression in Theorem 5 can be further simplified as follows.

Corollary 5.1: When $\alpha_{\mathrm{L}} = 2$, the SINR coverage probability approximately equals

$$P_{\mathrm{c}}(T) \approx \rho \mathrm{e}^{-\rho} \sum_{\ell=1}^{N} (-1)^{\ell+1} \binom{N}{\ell} \int_0^1 \prod_{k=1}^{4} \mathrm{e}^{\rho b_k \left(\mathrm{e}^{-\ell\eta T\bar{a}_k t} - t\mathrm{e}^{-\ell\eta T\bar{a}_k}\right)} \left(\frac{1-\mathrm{e}^{-\ell\mu\eta T\bar{a}_k t}}{1-\mathrm{e}^{-\ell\mu\eta T\bar{a}_k}} \right)^{\ell\eta T b_k \bar{a}_k t} \mathrm{d}t, \tag{18}$$

where $\mu = \mathrm{e}^{0.577}$.

The results in Theorem 5 generally provide a close approximation of the SINR distribution when enough terms are used, e.g. when $N \geq 5$, as will be shown in Section IV-D. More importantly, we note that the expressions in Theorem 6 are very efficient to compute, as most numerical tools support fast evaluation of the gamma function in (17), and (18) only requires a simple integral over a finite interval. Besides, given the path loss exponent α_{L} and the antenna geometry a_k, b_k, Theorem 5 shows that the approximated SINR is only a function of the relative density ρ, which indicates the SIR distribution in a dense network is mostly determined on the average number of LOS base station to a user.

C. Asymptotic Analysis in Ultra-Dense Networks

To obtain further insights into coverage in dense networks, we provide results on the asymptotic SIR distribution when the relative density ρ becomes large. We use this distribution to answer the following questions: (i) What is the asymptotic SIR distribution when the network becomes extremely dense? (ii) Does increasing base station density always improve SIR in a mmWave network?

First, we present the main asymptotic results as follows.

Theorem 6: In a dense network, when the LOS path loss exponent $\alpha_{\mathrm{L}} \leq 2$, the SIR converges to zero in probability, as $\rho \to \infty$. When $\alpha_{\mathrm{L}} > 2$, the SIR distribution converges to a nonzero

equivalence SIR_0, as $\rho \to \infty$. The distribution of the asymptotic equivalent SIR_0 is given in Proposition 10 of [30], and for $T > 1$, it follows that $\mathbb{P}(\text{SIR}_0 > T) = \frac{\alpha_{\text{L}} T^{-2/\alpha_{\text{L}}}}{2\pi \sin(2\pi/\alpha_{\text{L}})}$.

Proof: See Appendix E. ■

Note that Theorem 6 indicates that increasing base station density above some threshold will hurt the system performance, and that the base station density to achieve the optimal SINR is finite.

Now we provide an intuitive explanation of the asymptotic results as follows. When increasing the base station density, the distances between the user and base stations become smaller, and the user becomes more likely to be associated with a LOS base station. When the density is very high, however, a user sees several LOS base stations and thus experiences significant interference.

We note that the asymptotic trends in Theorem 6 are valid when base stations are all assumed to be active in the network. A simple way to avoid "over-densification" is to simply turn off a fraction of the base stations. This is a simple kind of interference management; study of more advanced interference management concepts is an interesting topic for future work.

D. Numerical Results

First, we illustrate the results in Theorem 5 with the simulations in Fig. 9. In the simulations, we include the NLOS base stations and thermal noise, which were ignored in the theoretical derivation. As illustrated in Fig. 9, the expression derived in Theorem 5 generally provides a lower bound of the coverage probability. The approximation becomes more accurate when more terms are used in the approximation, especially when $N \geq 5$. We find that the error due to ignoring NLOS base stations and thermal noise is minor in terms of the SINR coverage probability, primarily impacting low SINRs.

Next, we compare the SINR coverage probability with different relative base station density when $T = 20$ dB. Recall that $\rho = \lambda \pi R_{\text{B}}$ is the base station density normalized by the size of the LOS region. In 10(a), the path loss exponent is assumed to be $\alpha = 2$. We compute the coverage probability from $\rho = -20$ dB meters to $\rho = 20$ dB with a step of 1 dB. The analytical expressions in Theorem 5 are much more efficient than simulations: the plot takes seconds to finish using the analytical expression, while it approximately takes an hour to simulate 10,000 realizations at each step. As shown in Fig. 10 (a), although there is some gap between the simulation and the analytical results in the ultra-dense network regime, both curves achieve their

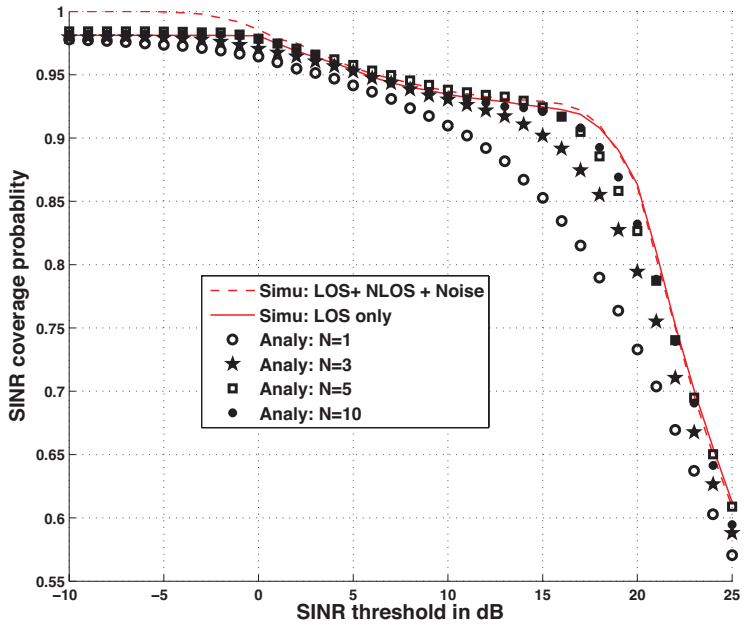

Fig. 9. Coverage probability in a dense mmWave network. The mmWave transmit antenna pattern is assumed to be $G_{10\text{dB},-10\text{dB},30^\circ}$. We assume $R_{\text{B}} = 200$ m, and the relative base station density $\rho = 4$. N is the number of terms we used to approximate the coverage probability in Theorem 5.

maxima at approximately $\rho = 5$, i.e., when the average cell radius r_c is approximately 1/2 of the LOS range R_{B}. Moreover, when the base station density grows very large, the coverage probability begins to decrease, which matches the asymptotic results in Theorem 6. The results also indicate that networks in the environments with dense blockages, e.g. the downtown areas of large cities where the LOS range R_{B} is small, will benefit from network densification; as they are mostly operated in the region where the relative density is (much) smaller than the optimal value $\rho \approx 5$, and thus increasing ρ by densifying networks will improve SINR coverage.

We also simulate with other LOS path loss exponents in Fig. 10 (b). The results show that the optimal base station density is generally insensitive to the change of the path loss exponent. When the LOS path loss exponent increases from 1.5 to 2.5, the optimal cell size is almost the same. The results also illustrate that the networks with larger path loss exponent α_{L} have better SINR coverage in the ultra-dense regime when $\rho > 10$. Intuitively, signals attenuate faster with a larger path loss exponent, and thus the inter-cell interference becomes weaker, which motivates a denser deployment of base stations in the network with higher path loss.

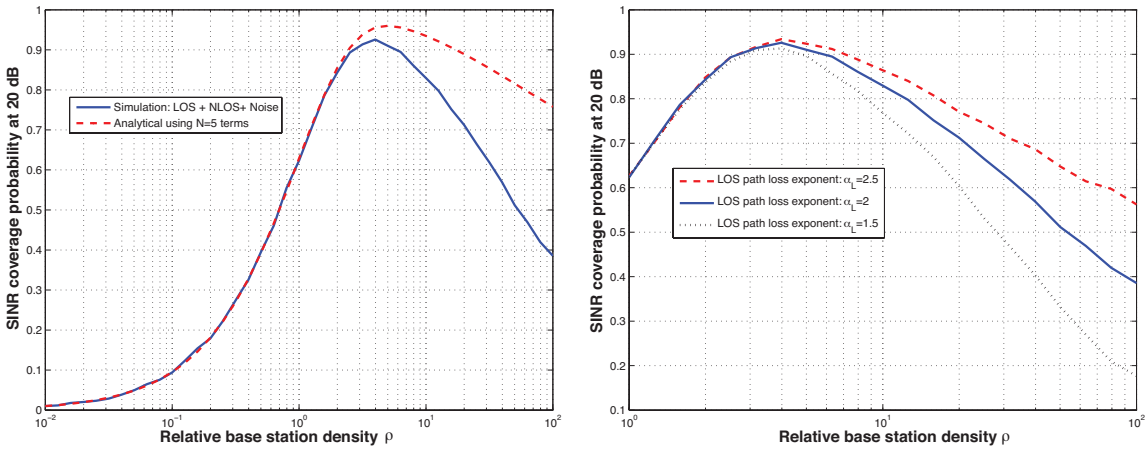
SINR coverage probability at 20 dB
Relative base station density ρ
Simulation: LOS + NLOS+ Noise
Analytical using N=5 terms
SINR coverage probability at 20 dB
Relative base station density ρ
LOS path loss exponent: α_L=2.5
LOS path loss exponent: α_L=2
LOS path loss exponent: α_L=1.5

(a) Analytical results using Theorem 5.

(b) Optimal density with different path loss exponents.

Fig. 10. SINR coverage probability with different relative base station density when the target SINR=20 dB. In the simulations, we include the NLOS base stations outside the LOS region and the thermal noise. We also fix the radius of the LOS ball as R_{B} =200 meters, and change the base station density λ at each step according to the value of the relative base station density ρ. In (a), it shows that ignoring NLOS base stations and the noise power causes minor errors in terms of the optimal cell radius. In (b), we search for the optimal relative density with different LOS path loss exponents. It shows that the optimal cell radius is generally insensitive to the path loss exponent.

TABLE II

ACHIEVABLE RATE WITH DIFFERENT BS DENSTIY

Base Station density	Ultra dense	Dense	Intermediate	Sparse	Microwave
Relative density ρ	16	4	1	0.45	-
Spectrum efficiency (bps/Hz)	5.5	5.8	4.3	2.7	4.6
Signal bandwith (MHz)	100	100	100	100	20
Achievable rate (Mpbs)	550	580	430	270	92

Finally, we compare the spectral efficiency and average achievable rates as a function of the relative density ρ in Table II. We find with a reasonable amount of density, e.g. when the relative density ρ is approximately 1, the mmWave system can provide comparable spectrum efficiency as the microwave system. With high density, rates that can be achieved are an order of magnitude better than microwave, due to the larger available bandwidth at mmWave frequencies.

V. Conclusions

In this paper, we proposed a stochastic geometry framework to analyze coverage and rate in mmWave networks. Our model took blockage effects into account by applying a distance-dependent LOS probability function, and modeling the base stations as independent inhomogeneous LOS and NLOS point processes. Based on the proposed framework, we derived expressions for the downlink SINR and rate coverage probability in mmWave cellular networks, which are shown to be efficient in computation and also a good fit with the simulations. We further simplified the blockage model by approximating the random LOS region as a fixed-size equivalent LOS ball. Applying the simplified framework, we analyzed the performance and asymptotic trends in dense networks.

We used numerical results to draw several important conclusions about coverage and rate in mmWave networks.

- SINR coverage can be comparable to microwave networks when the base station density is sufficiently high.
- Achievable rates can be significantly higher than in microwave networks, thanks to the larger available bandwidths.
- The SINR and rate performance is largely determined by the relative base station density, which is the ratio of the base station density to the blockage density. A transition from a power-limited regime to a interference-limited regime is also observed in mmWave networks, when increasing base station density.
- The optimal SINR and rate coverage can be achieved with a finite base station density; as increasing base station density need not improve SINR in a (ultra) dense mmWave network.

In future work, it would be interesting to analyze the networks with overlaid microwave macrocells, as mmWave systems will co-exist with microwave base stations. It would be another interesting topic to incorporate mmWave hardware constraints in the system analysis, and investigate the performance of mmWave networks applying analog/ hybrid beamforming [31] or using low-resolution A/D converters at the receivers [32].

Appendix A

We provide two useful inequalities in the following lemmas. The first lemma approximates the tail probability of a gamma random variable.

Lemma 6 (From [33]): Let g be a normalized gamma random variable with parameter N. For a constant $\gamma > 0$, the probability $\mathbb{P}(g < \gamma)$ can be tightly upper bounded by

$$\mathbb{P}(g < \gamma) < \left[1 - \mathrm{e}^{-a\gamma}\right]^N,$$

where $a = N(N!)^{-\frac{1}{N}}$.

The following inequality will be used in the dense network analysis.

Lemma 7 (From [33]): For $x > 0$, it holds that

$$-\log(1 - \mathrm{e}^{-ax}) \leq \int_x^\infty \frac{\mathrm{e}^{-t}}{t}\mathrm{d}t \leq -\log(1 - \mathrm{e}^{-bx}),$$

where $a = \mathrm{e}^{0.5772}$ and $b = 1$. Further, the lower bound generally provides a close approximation.

APPENDIX B

Proof of Lemma 2: For $s = \{\mathrm{L}, \mathrm{N}\}$, let d_s be the distance from the typical user to its nearest base station in Φ_s. The user is associated with a base station in Φ_L if and only if its nearest base station in Φ_L has smaller path loss than that of the nearest base station in Φ_N. Hence, it follows that

$$A_\mathrm{L} = \mathbb{P}\left(C_\mathrm{L} d_\mathrm{L}^{-\alpha_\mathrm{L}} > C_\mathrm{N} d_\mathrm{N}^{-\alpha_\mathrm{N}}\right) \overset{(a)}{=} \int_0^\infty \mathbb{P}\left(d_\mathrm{N} > \psi_\mathrm{L}(x)\right) f_\mathrm{L}(x)\mathrm{d}x. \tag{19}$$

where (a) follows that by Lemma 1, $f_\mathrm{L}(x)$ is the probability density function of d_L. Next, note that

$$\mathbb{P}\left(d_\mathrm{N} > \psi(x)\right) = \mathbb{P}\left(\Phi_\mathrm{N} \cup \mathcal{B}(0, \psi(x)_\mathrm{L}) = \emptyset\right) = \mathrm{e}^{-2\pi\lambda \int_0^{\psi_\mathrm{L}(x)} (1-p(t))t\mathrm{d}t}, \tag{20}$$

where $\mathcal{B}(0, x)$ denotes the ball centered at the origin of radius x. Substituting (20) for (19) gives Lemma 2. ■

APPENDIX C

Proof of Theorem 3: Given that the user is associated with a base station in Φ_L, the conditional coverage probability can be computed as

$$P_{\mathrm{c},1}(T) = \int_0^\infty \mathbb{P}_{h_\ell, \Phi}\left[h_0 M_\mathrm{r} M_\mathrm{t} x^{-\alpha_\mathrm{L}} > T\left(\sigma^2 + I_\mathrm{L} + I_\mathrm{N}\right)\right] \hat{f}_\mathrm{L}(x)\mathrm{d}x,$$

where $I_\mathrm{L} = \sum_{\ell: X_\ell \in \Phi_\mathrm{L} \cup \bar{\mathcal{B}}(0,x)} |h_\ell|^2 A_\ell R_\ell^{-\alpha_\mathrm{L}}$ and $I_\mathrm{N} = \sum_{\ell: X_\ell \in \Phi_\mathrm{N} \cup \bar{\mathcal{B}}(0,\psi(x))} |h_\ell|^2 A_\ell R_\ell^{-\alpha_\mathrm{N}}$ are the interference strength from the tiers of LOS and NLOS base stations, respectively. Next, noting that $|h_0|^2$ is a normalized gamma random variable with parameter N_L, we have the following approximation

$$\mathbb{P}_{h_\ell, \Phi}\left[h_0 M_\mathrm{r} M_\mathrm{t} x^{-\alpha_\mathrm{L}} > T\left(\sigma^2 + I_\mathrm{L} + I_\mathrm{N}\right)\right] \tag{21}$$

$$= \mathbb{P}_{h_0}\left[h_0 > x^{\alpha_{\mathrm{L}}} T\left(\sigma^2 + I_{\mathrm{L}} + I_{\mathrm{N}}\right)/(C_{\mathrm{L}} M_{\mathrm{r}} M_{\mathrm{t}})\right] \tag{22}$$

$$\overset{(a)}{\approx} 1 - \mathbb{E}_{\Phi}\left[\left(1 - \exp\left(-\frac{\eta_{\mathrm{L}} x^{\alpha_{\mathrm{L}}} T\left(\sigma^2 + I_{\mathrm{L}} + I_{\mathrm{N}}\right)}{C_{\mathrm{L}} M_{\mathrm{r}} M_{\mathrm{t}}}\right)\right)^{N_{\mathrm{L}}}\right] \tag{23}$$

$$\overset{(b)}{=} \sum_{n=1}^{N_{\mathrm{L}}} (-1)^{n+1} \binom{N_{\mathrm{L}}}{n} \mathbb{E}_{\Phi}\left[\exp\left(-\frac{n\eta_{\mathrm{L}} x^{\alpha_{\mathrm{L}}} T\left(\sigma^2 + I_{\mathrm{L}} + I_{\mathrm{N}}\right)}{C_{\mathrm{L}} M_{\mathrm{r}} M_{\mathrm{t}}}\right)\right] \tag{24}$$

$$\overset{(c)}{=} \sum_{n=1}^{N_{\mathrm{L}}} (-1)^{n+1} \binom{N_{\mathrm{L}}}{n} \mathrm{e}^{-\frac{n\eta_{\mathrm{L}} x^{\alpha_{\mathrm{L}}} T\sigma^2}{C_{\mathrm{L}} M_{\mathrm{r}} M_{\mathrm{t}}}} \mathbb{E}_{\Phi_{\mathrm{L}}}\left[\exp\left(-\frac{n\eta_{\mathrm{L}} x^{\alpha_{\mathrm{L}}} T I_{\mathrm{L}}}{C_{\mathrm{L}} M_{\mathrm{r}} M_{\mathrm{t}}}\right)\right] \mathbb{E}_{\Phi_{\mathrm{N}}}\left[\exp\left(-\frac{n\eta_{\mathrm{L}} x^{\alpha_{\mathrm{L}}} T I_{\mathrm{N}}}{C_{\mathrm{L}} M_{\mathrm{r}} M_{\mathrm{t}}}\right)\right] \tag{25}$$

where $\eta_{\mathrm{L}} = N_{\mathrm{L}}(N_{\mathrm{L}}!)^{-\frac{1}{N_{\mathrm{L}}}}$, (a) is from Lemma 6 [33] in Appendix A, (b) follows from Binomial theorem and the assumption that N_{L} is an integer, and (c) follows from the fact that Φ_{L} and Φ_{N} are independent. Now we apply concepts from stochastic geometry to compute the term $\mathbb{E}_{\Phi_{\mathrm{L}}}\left[\exp\left(-\frac{n\eta_{\mathrm{L}} x^{\alpha_{\mathrm{L}}} T I_{\mathrm{L}}}{C_{\mathrm{L}} M_{\mathrm{r}} M_{\mathrm{t}}}\right)\right]$ as

$$\mathbb{E}_{\Phi_{\mathrm{L}}}\left[\exp\left(-\frac{n\eta_{\mathrm{L}} x^{\alpha_{\mathrm{L}}} T I_{\mathrm{L}}}{C_{\mathrm{L}} M_{\mathrm{r}} M_{\mathrm{t}}}\right)\right] = \mathbb{E}\left[\exp\left(-\frac{n\eta_{\mathrm{L}} x^{\alpha_{\mathrm{L}}} T \sum_{\ell: X_\ell \in \Phi_{\mathrm{L}} \cup \bar{\mathcal{B}}(0,x)} |h_\ell|^2 A_\ell R_\ell^{-\alpha_{\mathrm{L}}}}{M_{\mathrm{r}} M_{\mathrm{t}}}\right)\right] \tag{26}$$

$$\overset{(c)}{=} \exp\left(-2\pi\lambda \sum_{k=1}^{4} b_k \int_x^{\infty} \left(1 - \mathbb{E}_g\left[\mathrm{e}^{-nT\eta_{\mathrm{L}} g \bar{a}_k (x/t)^{\alpha_{\mathrm{L}}}}\right]\right) p(t) t \mathrm{d}t\right) \tag{27}$$

$$\overset{(d)}{=} \prod_{k=1}^{4} \exp\left(-2\pi\lambda b_k \int_x^{\infty} \left(1 - 1/(1 + \eta_{\mathrm{L}} \bar{a}_k nT(x/t)^{\alpha_{\mathrm{L}}}/N_{\mathrm{L}})^{N_{\mathrm{L}}}\right) p(t) t \mathrm{d}t\right) \tag{28}$$

$$= \mathrm{e}^{-Q_n(T,x)}, \tag{29}$$

where g in (c) is a normalized gamma random variable with parameter N_{L}, $\bar{a}_k = \frac{a_k}{M_{\mathrm{t}} M_{\mathrm{r}}}$, and for $1 \le k \le 4$, a_k and b_k are defined previously in Table I; (c) is from computing the Laplace functional of the PPP Φ_{L} [26]; (d) is by computing the moment generating function of a gamma random variable g.

Similarly, we can compute $\mathbb{E}_{\Phi_{\mathrm{N}}}\left[\exp\left(-\frac{n\eta_{\mathrm{L}} x^{\alpha_{\mathrm{L}}} T I_{\mathrm{N}}}{C_{\mathrm{L}} M_{\mathrm{r}} M_{\mathrm{t}}}\right)\right]$ as

$$\mathbb{E}\left[\exp\left(-\frac{n\eta_{\mathrm{L}} x^{\alpha_{\mathrm{L}}} T I_{\mathrm{N}}}{C_{\mathrm{L}} M_{\mathrm{r}} M_{\mathrm{t}}}\right)\right] = \mathbb{E}\left[\exp\left(-\frac{n\eta_{\mathrm{L}} x^{\alpha_{\mathrm{L}}} T C_{\mathrm{N}} \sum_{\ell: X_\ell \in \Phi_{\mathrm{N}} \cup \bar{\mathcal{B}}(0,\psi(x))} |h_\ell|^2 A_\ell R_\ell^{-\alpha_{\mathrm{N}}}}{C_{\mathrm{L}} M_{\mathrm{r}} M_{\mathrm{t}}}\right)\right] \tag{30}$$

$$= \prod_{k=1}^{4} \exp\left(-2\pi\lambda b_k \int_{\psi_{\mathrm{L}}(x)}^{\infty} \left(1 - 1/(1 + \eta_{\mathrm{L}} \bar{a}_k nTC_{\mathrm{N}} x^{\alpha_{\mathrm{L}}}/(C_{\mathrm{L}} t^{\alpha_{\mathrm{N}}} N_{\mathrm{N}}))^{N_{\mathrm{N}}}\right) (1 - p(t))\, t \mathrm{d}t\right) \tag{31}$$

$$= \mathrm{e}^{-V_n(T,x)}. \tag{32}$$

Then, we obtain (9) by the linearity of integrals.

Given the user is associated with a NLOS base station, we can also derive the conditional coverage probability $P_{c,2}(T)$ following same approach as that of $P_{c,1}(T)$. Thus, we omit the detailed proof of (10) here.

Finally, by the law of total probability, it follows that $P_{\rm c}(T) = A_{\rm L}P_{\rm c,1}(T) + A_{\rm N}P_{\rm c,2}(T)$. ■

APPENDIX D

Proof of Theorem 5 For a general $\alpha_{\rm L}$, the coverage probability can be computed as

$$P_{\rm c}(T) = A_{\rm L}P_{\rm c}(T) = A_{\rm L}\mathbb{P}(\text{SIR} > T) = A_{\rm L}\int_0^{R_{\rm B}} \mathbb{P}(C_{\rm L}M_rM_tr^{-\alpha_{\rm L}} > TI_r)\frac{2\pi\lambda r}{A_{\rm L}}\mathrm{e}^{-\lambda\pi r^2}\mathrm{d}r, \tag{33}$$

where $I_r = \sum_{X_\ell\in\Phi\cap\mathcal{B}(r,R_{\rm B})} A_\ell C_{\rm L} R_\ell^{-\alpha_{\rm L}}$ is the interference power given that the distance to the user's serving base station is $R_0 = r$. Also, the probability $\mathbb{P}(M_rM_tr^{-\alpha_{\rm L}} > TI_r)$ can be approximated as

$$\mathbb{P}(C_{\rm L}M_rM_tr^{-\alpha_{\rm L}} > TI_r) \overset{(a)}{\approx} \mathbb{P}(g > Tr^{\alpha_{\rm L}}I_r/(C_{\rm L}M_rM_t)) \tag{34}$$

$$\overset{(b)}{\approx} 1 - \mathbb{E}_{\Phi_{\rm L}}\left[\left(1-\mathrm{e}^{-\eta Tr^{\alpha_{\rm L}}I_r/(C_{\rm L}M_rM_t)}\right)^N\right] \tag{35}$$

$$= \sum_{\ell=1}^{N}\binom{N}{\ell}(-1)^\ell \mathbb{E}_{\Phi_{\rm L}}\left[\mathrm{e}^{-\ell\eta Tr^{\alpha_{\rm L}}I_r/(C_{\rm L}M_rM_t)}\right]. \tag{36}$$

In (a), the dummy variable g is a normalized gamma variable with parameter N, and the approximation in (a) follows from the fact that a normalized Gamma distribution converges to identity when its parameter goes to infinity, i.e., $\lim_{n\to\infty}\frac{n^nx^{n-1}\mathrm{e}^{-nx}}{\Gamma(n)} = \delta(x-1)$ [34], where $\delta(x)$ is the Dirac delta function. In (b), it directly follows from Lemma 6 by taking $\eta = N(N!)^{1/N}$.

Next, we can compute $\mathbb{E}_{\Phi_{\rm L}}\left[\mathrm{e}^{-\ell\eta Tr^{\alpha_{\rm L}}I_r/(C_{\rm L}M_rM_t)}\right]$ as

$$\mathbb{E}_{\Phi_{\rm L}}\left[\mathrm{e}^{-\ell\eta Tr^{\alpha_{\rm L}}I_r/(M_rM_t)}\right] \overset{(c)}{=} \exp\left(\sum_{k=1}^{4} -2\pi\lambda b_k\int_r^{R_{\rm B}} 1-\mathrm{e}^{-\ell\eta\bar{a}_kT(r/t)^{\alpha_{\rm L}}}t\mathrm{d}t\right) \tag{37}$$

$$\overset{(d)}{=} \mathrm{e}^{-\pi\lambda(R_{\rm B}^2-r^2)}\exp\left(\sum_{k=1}^{4}\frac{2}{\alpha_{\rm L}}\pi\lambda b_k(T\ell\eta\bar{a}_k)^{2/\alpha_{\rm L}}\int_{\ell\eta T\bar{a}_k(r/R_{\rm B})^{\alpha_{\rm L}}}^{\ell\eta T\bar{a}_k}\frac{\mathrm{e}^{-s}}{s^{1+2/\alpha_{\rm L}}}\mathrm{d}s\right) \tag{38}$$

$$= \mathrm{e}^{-\pi\lambda(R_{\rm B}^2-r^2)}\exp\left(\sum_{k=1}^{4}\frac{2}{\alpha_{\rm L}}\pi\lambda b_k(T\ell\eta\bar{a}_k)^{2/\alpha_{\rm L}}\Gamma\left(\frac{-2}{\alpha_{\rm L}};\ell\eta T\bar{a}_k(r/R_{\rm B})^{\alpha_{\rm L}},\ell\eta T\bar{a}_k\right)\right), \tag{39}$$

where (c) follows from computing the Laplace functional of the PPP $\Phi_{\rm L}$ [26], and (d) follows from changing variable as $s = \ell\eta\bar{a}_kT(r/t)^{\alpha_{\rm L}}$. Hence,(17) directly follows from substituting (39) for (33) and letting $\rho = 2\pi\lambda R_{\rm B}^2$.

When $\alpha_{\rm L} = 2$, the steps above hold true till (38), which can be further simplified as

$$\mathbb{E}_{\Phi_{\rm L}}\left[\mathrm{e}^{-\ell\eta Tr^{\alpha_{\rm L}}I_r/(M_rM_t)}\right] = \mathrm{e}^{-\pi\lambda(R_{\rm B}^2-r^2)}\exp\left(\sum_{k=1}^{4}\pi\lambda b_kT\ell\eta\bar{a}_k\int_{\ell\eta T\bar{a}_k(r/R_{\rm B})^2}^{\ell\eta T\bar{a}_k}\frac{\mathrm{e}^{-s}}{s^2}\mathrm{d}s\right) \tag{40}$$

$$\overset{(e)}{=} \mathrm{e}^{-\pi\lambda(R_{\mathrm{B}}^2-r^2)} \exp\left(-\sum_{k=1}^{4}\pi\lambda b_k\left(\mathrm{e}^{-\ell T\ell\eta\bar{a}_k}-\frac{\mathrm{e}^{-(r/R_{\mathrm{B}})^2\ell T\ell\eta\bar{a}_k}}{(r/R_{\mathrm{B}})^2}+\int_{\ell T\ell\eta\bar{a}_k(r/R_{\mathrm{B}})^2}^{\ell T\ell\eta\bar{a}_k}\frac{\mathrm{e}^{-s}}{s}\mathrm{d}s\right)\right) \tag{41}$$

$$\overset{(f)}{\approx} \mathrm{e}^{-\pi\lambda(R_{\mathrm{B}}^2-r^2)} \exp\left(-\sum_{k=1}^{4}\pi\lambda b_k\left(\mathrm{e}^{-\ell T\ell\eta\bar{a}_k}-\frac{\mathrm{e}^{-(r/R_{\mathrm{B}})^2\ell T\ell\eta\bar{a}_k}}{(r/R_{\mathrm{B}})^2}+\log\frac{1-\mathrm{e}^{\mu\ell T\ell\eta\bar{a}_k(r/R_{\mathrm{B}})^2}}{1-\mathrm{e}^{\mu\ell T\ell\eta\bar{a}_k}}\right)\right), \tag{42}$$

where (e) is from computing integration by part, (f) follows from Lemma 7 by letting $\mu = \mathrm{e}^{0.5772}$. Lastly, (18) follows from substituting (42) for (33) and letting $\rho = 2\pi\lambda R_{\mathrm{B}}^2$. ■

APPENDIX E

Proof Sketch of Theorem 6: First, we show that the exact SIR distribution in our dense network model is unchanged when the relative density $\rho = \lambda\pi R_{\mathrm{B}}^2$ is fixed. Let $F_\ell = R_\ell^{\alpha_{\mathrm{L}}}$ be the path loss gain in the ℓ-th link. Then the SIR expression in (16) can be rewritten as $\mathrm{SIR} = A_0F_0^{-1}/\left(\sum_{\ell:X_\ell\in\Phi_{\mathrm{L}}}A_\ell F_\ell^{-1}\right)$, where A_ℓ is determined by the geometries of the antenna arrays. Further, using displacement theorem [26] and the method in [1, Lemma 7], we can show that $\{F_\ell\}_{\ell:X_\ell\in\Phi_{\mathrm{L}}}$ forms a PPP on the interval $(0, R_{\mathrm{B}}^{\alpha_{\mathrm{L}}})$ with density measure function $\Lambda(0,t) = \lambda\pi t^{2/\alpha_{\mathrm{L}}}$. For $c > 0$, we define an *alternative network* with base station density $c\lambda$ and LOS range $c^{-0.5}R_B$, which give the same relative density $\rho = \lambda\pi R_{\mathrm{B}}^2$ as the original network. We can also show that a scaled version of path loss gain process $\left\{c^{\alpha_{\mathrm{L}}/2}F_\ell\right\}_\ell$ in the alternative network has the exact same distribution as $\{F_\ell\}_\ell$ in the original network. Thus, the alternative network has the same SIR distribution as the original network; as the SIR also equals $A_0c^{-\alpha_{\mathrm{L}}/2}F_0^{-1}/\left(\sum_{\ell:X_\ell\in\Phi_{\mathrm{L}}}A_\ell c^{-\alpha_{\mathrm{L}}/2}F_\ell^{-1}\right)$. Equivalently, we have shown that the SIR distribution in dense networks is unchanged when the relative density ρ is fixed.

Next, note that letting $\rho\to\infty$ is equivalent to fixing λ as a constant λ_0 and letting $R_{\mathrm{B}}\to\infty$. Hence, when $\rho\to\infty$, the asymptotic equivalent SIR has the same distribution as the SIR in its *asymptotic equivalent network*, where LOS base stations form a homogeneous PPP with density λ_0 on the entire plane. For $\alpha_{\mathrm{L}} > 2$, the distribution of the equivalent SIR can be computed through Proposition 10 in [30].

Finally, we show that the SIR converges to zero the asymptotic equivalent network, when $\alpha_{\mathrm{L}} \le 2$. By [35, Proposition 1, Fact 1], the SIR in the asymptotic equivalent network is invariant with the small-scale fading distribution, and thus is same as the distribution in the *Rayleigh-fading network* in [18], where independent Rayleigh fading is assumed in each links. The SIR in the Rayleigh-fading network can be upper bounded as follows. For $\forall T > 0$,

$$P_{\mathrm{c}}(T) = \mathbb{P}\left[\bigcup_{X_\ell\in\Phi_{\mathrm{L}}}\mathrm{SIR}(X_\ell) > T\right] \tag{43}$$

$$\overset{(a)}{\leq} \sum_{X_\ell \in \Phi_{\mathrm{L}}} \mathbb{P}\left[\mathrm{SIR}(X_\ell) > T\right] \tag{44}$$

$$\overset{(b)}{=} \pi\lambda \int_0^\infty \exp\left(-\pi\lambda T^{2/\alpha_{\mathrm{L}}} t \int_0^\infty \frac{1}{1+r^{\alpha_{\mathrm{L}}/2}} \mathrm{d}r\right) \mathrm{d}t \tag{45}$$

$$= \frac{T^{-2/\alpha_{\mathrm{L}}}}{\int_0^\infty \frac{1}{1+r^{\alpha_{\mathrm{L}}/2}} \mathrm{d}r} \tag{46}$$

$$\overset{(c)}{=} 0, \tag{47}$$

where $\mathrm{SIR}(X_\ell)$ is the SIR given the user is connected to the ℓ-th base station of Φ_{L}, (a) is from the union bound, (b) follows from the similar algebra in [18, Appendix B, Eqn (15)-(17)], and (c) is from the fact that $\int_0^\infty \frac{1}{1+r^{\alpha_{\mathrm{L}}/2}} \mathrm{d}r$ is infinity when $\alpha_{\mathrm{L}} \leq 2$. Hence, the SIR distribution in the Rayleigh network is zero with probability one, and so is the SIR distribution in the asymptotic equivalent network, which also equivalently means that the SIR distribution in the original network converges to zero in probability when $\rho \to \infty$. ■

REFERENCES

[1] T. Bai and R. W. Heath Jr., "Coverage analysis for millimeter wave cellular networks with blockage effects," in *Proc. of IEEE Global Conf. on Signal and Information Processing (GlobalSIP)*, Dec. 2013.

[2] ——, "Coverage in dense millimeter wave cellular networks," in *Proc. of the Forty Seventh Asilomar Conf. on Signals, Systems and Computers (ASILOMAR)*, Nov. 2013, pp. 1–5.

[3] T. S. Rappaport, R. W. Heath Jr., R. C. Daniels, and J. N. Murdock, *Millimeter Wave Wireless Communication*. Prentice Hall, 2014.

[4] Z. Pi and F. Khan, "An introduction to millimeter-wave mobile broadband systems," *IEEE Commun. Mag.*, vol. 49, no. 6, pp. 101 –107, Jun. 2011.

[5] T. Rappaport *et al.*, "Millimeter wave mobile communications for 5G cellular: It will work!" *IEEE Access*, vol. 1, pp. 335–349, 2013.

[6] T. Baykas *et al.*, "IEEE 802.15.3c: the first IEEE wireless standard for data rates over 1 Gb/s," *IEEE Commun. Mag.*, vol. 49, no. 7, pp. 114–121, 2011.

[7] IEEE, "IEEE Standard - Part 11: Wireless LAN MAC and PHY Specifications Amendment 3: Enhancements for Very High Throughput in the 60 GHz Band," 2012.

[8] ——, "IEEE Standard for WirelessMAN-Advanced Air Interface for Broadband Wireless Access Systems," 2012.

[9] T. Rappaport *et al.*, "Broadband millimeter-wave propagation measurements and models using adaptive-beam antennas for outdoor urban cellular communications," *IEEE Trans. on Antennas Propag.*, vol. 61, no. 4, pp. 1850–1859, Apr. 2013.

[10] A. Goldsmith, *Wireless Communications*. Cambridge University Press, 2005.

[11] A. Alejos *et al.*, "Measurement and analysis of propagation mechanisms at 40 GHz: Viability of site shielding forced by obstacles," *IEEE Trans.Veh. Technol.*, vol. 57, no. 6, pp. 3369–3380, 2008.

[12] S. Rajagopal, S. Abu-Surra, and M. Malmirchegini, "Channel feasibility for outdoor non-line-of-sight mmwave mobile communication," in *Proc. of IEEE Veh. Technol. Conf. (VTC Fall)*, 2012, pp. 1–6.

[13] 3GPP TR 36.814, “Further advancements for E-UTRA physical layer aspects (Release 9),” Mar. 2010.

[14] M. Riza Akdeniz, Y. Liu, S. Sun, S. Rangan, T. S. Rappaport, and E. Erkip, “Millimeter Wave Channel Modeling and Cellular Capacity Evaluation,” Dec. 2013. [Online]. Available: http://arxiv.org/abs/1312.4921

[15] M. R. Akdeniz *et al.*, “Millimeter wave picocellular system evaluation for urban deployments,” *arXiv preprint arXiv:1304.3963*, 2013.

[16] J. G. Andrews, F. Baccelli, and R. Krishna Ganti, “A tractable approach to coverage and rate in cellular networks,” *IEEE Transactions on Communications*, vol. 59, no. 11, pp. 3122–3134, November 2011.

[17] A. Ghosh *et al.*, “Heterogeneous cellular networks: From theory to practice,” *IEEE Communications Magazine*, vol. 50, no. 6, pp. 54–64, Jun. 2012.

[18] H. S. Dhillon *et al.*, “Modeling and analysis of K-tier downlink heterogeneous cellular networks,” *IEEE Journal on Selected Areas in Communications*, vol. 30, no. 3, pp. 550–560, April 2012.

[19] R. W. Heath Jr. *et al.*, “Modeling heterogeneous network interference with using poisson point processes,” *To appear in IEEE Trans. Signal Processing*, April 2013. [Online]. Available: http://arxiv.org/abs/1207.2041

[20] S. Akoum, E. O. Ayach, and R. W. Heath Jr., “Coverage and capacity in mmWave cellular systems,” in *Proc. of the Forty Sixth Asilomar Conf. on Signals, Systems and Computers (ASILOMAR)*, 2012, pp. 688–692.

[21] S. Seidel and T. Rappaport, “Site-specific propagation prediction for wireless in-building personal communication system design,” *IEEE Trans. Veh. Technol.*, vol. 43, no. 4, pp. 879–891, 1994.

[22] A. Toscano, F. Bilotti, and L. Vegni, “Fast ray-tracing technique for electromagnetic field prediction in mobile communications,” *IEEE Trans. on Magnetics*, vol. 39, no. 3, pp. 1238–1241, May 2003.

[23] M. Franceschetti, J. Bruck, and L. Schulman, “A random walk model of wave propagation,” *IEEE Trans. Antennas Propag.*, vol. 52, no. 5, pp. 1304–1317, 2004.

[24] T. Bai, R. Vaze, and R. W. Heath Jr., “Analysis of blockage effects on urban cellular networks,” *Submitted to IEEE Trans.Wireless Commun.*, Aug. 2013. [Online]. Available: arxiv.org/abs/1309.4141

[25] A. Hunter, J. Andrews, and S. Weber, “Transmission capacity of ad hoc networks with spatial diversity,” *IEEE Trans. Wireless Commun.*, vol. 7, no. 12, pp. 5058–5071, December 2008.

[26] F. Baccelli and B. Blaszczyszyn, *Stochastic Geometry and Wireless Networks, Volume I - Theory*. NOW Publishers, 2009.

[27] L. Greenstein and V. Erceg, “Gain reductions due to scatter on wireless paths with directional antennas,” *IEEE Commun. Let.*, vol. 3, no. 6, pp. 169–171, 1999.

[28] S. Singh, H. Dhillon, and J. Andrews, “Offloading in heterogeneous networks: Modeling, analysis, and design insights,” *Wireless Communications, IEEE Transactions on*, vol. 12, no. 5, pp. 2484–2497, May 2013.

[29] T. Bai, A. Alkhateeb, and R. W. Heath Jr, “Coverage and capacity in millimeter wave cellular networks,” *Submitted to IEEE Commun. Mag.*, Feb. 2014.

[30] B. Blaszczyszyn, M. K. Karray, and H. P. Keeler, “Using Poisson processes to model lattice cellular networks,” in *Prof. of IEEE International Conference on Computer Communications (INFOCOM)*, 2013.

[31] O. E. Ayach, S. Rajagopal, S. Abu-Surra, Z. Pi, and R. W. Heath Jr, “Spatially sparse precoding in millimeter wave MIMO systems,” *To appear in IEEE Trans. Wireless Commun.*, 2013. [Online]. Available: http://arxiv.org/abs/1305.2460

[32] J. Mo and R. W. Heath Jr., “High SNR capacity of millimeter wave MIMO systems with one-bit quantization,” in *Proc. of Information Theory and Applications (ITA)*, Feb. 2014.

[33] H. Alzer, “On some inequalities for the incomplete Gamma function,” *Mathematics of Computation*, vol. 66, no. 218, pp. 771–778, 1997. [Online]. Available: http://www.jstor.org/stable/2153894

[34] R. Aris, *Mathematical Modeling: A Chemical Engineer's Perspective*. Academic Press, 1999.

[35] X. Zhang and M. Haenggi, "The performance of successive interference cancellation in random wireless networks," *Submitted to IEEE Trans. Information Theory*, 2013. [Online]. Available: http://www3.nd.edu/~mhaenggi/pubs/tit14.pdf